



**HAL**  
open science

## A mechanistic surface complexation approach for the prediction of rare earth element reactive transport in quartz porous media

Muqet Iqbal, Rémi Marsac, Mélanie Davranche, Aline Dia, Khalil Hanna

### ► To cite this version:

Muqet Iqbal, Rémi Marsac, Mélanie Davranche, Aline Dia, Khalil Hanna. A mechanistic surface complexation approach for the prediction of rare earth element reactive transport in quartz porous media. *Chemical Geology*, 2023, 634, pp.121601. 10.1016/j.chemgeo.2023.121601 . insu-04132399

**HAL Id: insu-04132399**

**<https://insu.hal.science/insu-04132399>**

Submitted on 19 Jun 2023

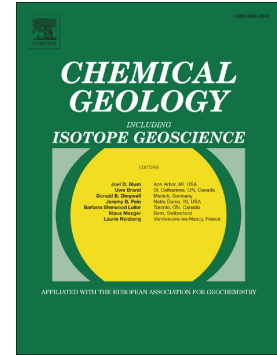
**HAL** is a multi-disciplinary open access archive for the deposit and dissemination of scientific research documents, whether they are published or not. The documents may come from teaching and research institutions in France or abroad, or from public or private research centers.

L'archive ouverte pluridisciplinaire **HAL**, est destinée au dépôt et à la diffusion de documents scientifiques de niveau recherche, publiés ou non, émanant des établissements d'enseignement et de recherche français ou étrangers, des laboratoires publics ou privés.

## Journal Pre-proof

A mechanistic surface complexation approach for the prediction of rare earth element reactive transport in quartz porous media

Muqet Iqbal, Rémi Marsac, Mélanie Davranche, Aline Dia, Khalil Hanna



PII: S0009-2541(23)00301-7

DOI: <https://doi.org/10.1016/j.chemgeo.2023.121601>

Reference: CHEMGE 121601

To appear in: *Chemical Geology*

Received date: 23 December 2022

Revised date: 11 June 2023

Accepted date: 14 June 2023

Please cite this article as: M. Iqbal, R. Marsac, M. Davranche, et al., A mechanistic surface complexation approach for the prediction of rare earth element reactive transport in quartz porous media, *Chemical Geology* (2023), <https://doi.org/10.1016/j.chemgeo.2023.121601>

This is a PDF file of an article that has undergone enhancements after acceptance, such as the addition of a cover page and metadata, and formatting for readability, but it is not yet the definitive version of record. This version will undergo additional copyediting, typesetting and review before it is published in its final form, but we are providing this version to give early visibility of the article. Please note that, during the production process, errors may be discovered which could affect the content, and all legal disclaimers that apply to the journal pertain.

© 2023 Published by Elsevier B.V.

***A mechanistic surface complexation approach for the prediction of rare earth element reactive transport in quartz porous media***

MUQEET IQBAL<sup>1</sup>, RÉMI MARSAC<sup>1\*</sup>, MÉLANIE DAVRANCHE<sup>1</sup>, ALINE DIA<sup>1</sup>, AND KHALIL HANNA<sup>2</sup>

<sup>1</sup>Univ Rennes, CNRS, Géosciences Rennes, UMR 6118, 35000 Rennes, France

<sup>2</sup>Univ Rennes, Ecole Nationale Supérieure de Chimie de Rennes, CNRS, ISCR-UMR 6226, F-35000, Rennes, France

(\*correspondence: remi.marsac@cnrs.fr)

Journal Pre-proof

**Abstract.** Although rare earth elements (REE) are now considered as emerging contaminants, the mechanisms controlling the mobility of REE in geochemical systems remain elusive. The complexity and multi-element characteristics of REE including potential synergistic and antagonistic interactions with environmental surfaces make the prediction of REE fate in nature a challenging task. In this study, a comprehensive set of batch and column transport experiments were conducted to examine the interactions of REE group, as well as some co-occurring or chemically analogous elements (Sc, Y, Th and U), with 100-300  $\mu\text{m}$  quartz sand particles. Results from batch experiments showed that middle REE (MREE) and heavy REE (HREE) are preferentially adsorbed at low and high REE loadings, which showed the occurrence of two different types of binding sites. A surface complexation model (SCM) has been developed, which successfully predicted sorption of REE, Sc, Y, Th and U. Experimental and reactive transport modeling evidenced the importance of the strong sites, and highlighted the competitive binding of MREE with other REE and Y for the quartz surface sites. These results may have strong implications for the development of new prediction tools for accurately assessing the reactive transport of REE in natural systems.

**Keywords:** rare earth elements; quartz; binding; mobility; modeling.

## 1 Introduction

Rare earth elements (REE) are a group of fourteen co-occurring elements (lanthanum, cerium, praseodymium, neodymium, samarium, europium, gadolinium, terbium, dysprosium, holmium, erbium, thulium, ytterbium, and lutetium) in surface environments. Their unique magnetic, optical and catalytic properties make them extremely interesting for many applications such as hybrid vehicles, wind turbines, laptops and smartphones (Anastopoulos et al., 2016; Drobniak and Mastalerz, 2022). Thus, the demand and the production of these critical metals have surged over the past decades (Li et al., 2016), which led to rising environmental concerns about their potential toxic effects on human health and ecosystems (Langkau and Erdmann, 2020). Therefore, to assess the ecological impacts of these emerging contaminants, it is necessary to investigate REE transport mechanisms in natural ecosystems.

Adsorption is recognized as one of the key processes governing the transport of REE in porous natural systems (Henderson, 1984). Quartz being often considered as a representative adsorbent in porous media due to its abundance and chemical stability, several studies investigated sorption of REE onto quartz (Fairhurst et al., 1995; Kitamura et al., 1999; Tang and Johannesson, 2005, 2010; Pitois et al., 2008; Kar et al., 2011; Jin et al., 2014; Schnurr et al., 2015; García et al., 2019; Karimzadeh et al., 2020). However, the most of these studies focused on a single or a few REE although they generally co-occur in natural systems and might compete with each other for adsorption processes. In addition, multi-REE investigations are particularly interesting due to the coherent evolution of their chemical behaviour with the atomic number: “REE patterns”, which can be obtained in adsorption studies by plotting the adsorbed amount onto particles against their atomic number. REE are often considered analogues as they have similar geochemical behavior and mainly exist as trivalent cations, except for Ce(III) which can be oxidized to Ce(IV) and Eu(III) which can be reduced to Eu(II) (Ohta and Kawabe, 2001; Davranche et al., 2005; Liu et al., 2017). REE patterns have been shown to probe surface complexation processes onto heterogeneous surfaces of organic composition such as natural organic colloids (Marsac et al., 2010, 2013; Catrouillet et al., 2019), bacterial cells (Takahashi et al., 2005, 2010), algae (Zoll and Schijf, 2012), and nanoplastics (Blanco et al., 2022). Furthermore, inorganic particles with homogeneous composition can exhibit different binding sites for metal ions, which leads to different REE patterns depending on the physico-chemical conditions, such as in the case of iron hydroxides (Quinn et al., 2004) or manganese oxides (Pourret and Davranche, 2013). The impact of site heterogeneity on REE patterns at the quartz surface has not been investigated yet, although the results of two recent studies on single REE (García et al., 2019; Amiel et al., 2022) suggest the occurrence of two surface sites.

In most of the listed above studies have used the valuable information provided by REE patterns to develop mechanistic surface complexation models (SCM). These models include detail understanding of ions binding at the adsorbing surface-water interface and can predict ion adsorption under various conditions, which includes surface site heterogeneity, pH, ionic strength and the presence of other ions inducing competitive or cooperative adsorption processes (Xu et al., 2017; Cheng et al., 2019). Mechanistic SCM can further be coupled with transport equation and can be valuable tools to account for these various effects on adsorption in both geochemical speciation and reactive transport modelling

studies of contaminants in the environmental systems (Cheng et al., 2019; Zhou et al., 2022; Luo et al., 2022). However, if column transport studies of REE in quartz sand is scarce, and mainly focused on a single or few REE (Nagao et al., 1998; Warwick et al., 2000; Bryan et al., 2005; Yoshida and Suzuki, 2006; Wang et al., 2020; Amiel et al., 2022), mechanistic SCM have also rarely been applied in reactive transport modeling investigation of REE. Hence, it is important to develop a reactive transport model to correlate molecular interactions of multi-element REE in static conditions with their macroscopic transport in flow-through conditions.

In natural conditions, other elements might compete with REE. For instance, in Earth's crust, REE exist in ores and minerals together with other metals such as scandium, yttrium and naturally occurring actinides such as thorium and uranium (Kursun et al., 2016). Particularly, the chemical behaviour of Y is very similar to Ho and therefore, is often included in the lanthanide series (as "REY") (e.g. Bau, 1999; Quinn et al., 2004; Pack et al., 2007). Sc is trivalent and its chemical behaviour is often compared to that of REE, although it exhibits a much smaller ionic radius (Balaram, 2012). U is a redox sensitive element, with oxidation states ranging from +4 to +6 in natural systems (Geckeis et al., 2013; Altmaier et al., 2013). It mainly occurs as uranyl ion ( $\text{UO}_2^{2+}$ ) in oxidizing conditions, which behaves as a cation with an effective charge of +3.3 (Choppin and Rao, 1984; Geckeis et al., 2013), close to that of REE. Th is a tetravalent element, which is often considered as analogous to other tetravalent actinides (e.g. U/Np/Pu(IV)) and Ce(IV) (Marsac et al., 2015, 2017). Therefore, multi-element studies on REE might also be extended to Sc, Y, Th and U for their comparative transport behaviour, but also because of their competitive effects on REE surface complexation to mineral particles.

In this study, the interactions of the REY group along with Sc, Th and U with 100-300  $\mu\text{m}$  Fontainebleau quartz sand particles were thoroughly examined under batch and dynamic flow-through conditions. In natural systems, the aqueous concentration and fractionation of REY is highly pH-dependent, therefore, experiments were conducted under a wide range of pH (3-7) and metal concentrations (1 and 5  $\mu\text{g L}^{-1}$ ), as well as under dynamic flow conditions. These experiments involved multi-metal ion conditions in order to (i) account for their competition for quartz surface sites and (ii) test the capability of REE adsorption patterns to probe the surface site heterogeneity of quartz particles. Different binding mechanisms were expected to occur depending on the experimental physical and chemical conditions, which should lead to REE-quartz pattern variability. The experimental metal ions adsorption data and, especially REE patterns, were then utilized to build a new surface complexation model (SCM) that can predict multi-metal ion pH and concentration-dependence. This knowledge is implemented to develop a reactive transport model that can simulate multi-metal ion transport in flow-through systems.

## 2 Materials and Methods

### 2.1 Material

To ensure the purity of the materials, analytical grade chemicals were used. The REE stock solution including Sc, Y, Th and U (10  $\text{mg L}^{-1}$  multi-element) was purchased from Inorganic Ventures. The solutions were prepared in containers cleaned with 10% (v/v)  $\text{HNO}_3$  for 24 h at 45 °C followed by soaking and rinsing with ultrapure water (18.2  $\Omega$ , MilliQ system, Millipore) for another 24 h at 45 °C to minimize metal ions contamination. All experiments were conducted at room temperature.

Fontainebleau quartz sand (100-300  $\mu\text{m}$ ) was purchased from Carlo Erba. The cleaning protocol for the sand was previously described (Scheidegger et al., 1993; Hanna et al., 2014). Briefly, 1M HCl was used to clean the quartz sand for 48 hours followed by rinsing with ultrapure water. Then the quartz sand was treated with  $\text{H}_2\text{O}_2$  to remove any organic matter contamination followed by ultrapure water. Finally, the quartz sand was oven-dried at 100 °C for 24 h and rinsed repeatedly with ultrapure water. A blank experiment was made with 2 %  $\text{HNO}_3$  and quartz sand, no REE were detected.

## 2.2 Batch experiments

The batch sorption experiments were carried out in 250 mL HDPE opaque reactors. The experiments were conducted by adding 1 g of quartz sand in a 100 mL of a solution containing REE, Sc, Y, Th and U simultaneously in 5 mM NaCl as a background electrolyte. The pH of the solutions was adjusted to the desired value by adding small volumes of HCl or NaOH (0.1 M) solutions. The pH meter (HACH Sension + PH1) used was calibrated using the buffer solution of pH 4, 7 and 10. This calibration was made every day before a series of pH adjustment or measurement of samples. After a given reaction time, the pH was measured and an aliquot of the supernatant is taken for REE concentration determination. No phase separation was required (e.g. filtration or centrifugation), because of the large size of sand particles, which sediment very rapidly.

Two sets of experiments were conducted at various pH values, with 1 and 5  $\mu\text{g L}^{-1}$  of each metal ion, which corresponds to total metal ion concentration ( $[M]$ ) of  $10^{-7}$  M and  $7 \times 10^{-7}$  M, respectively. The kinetic experiment was conducted for a period of 24 hours, during which sampling was performed at regular intervals. In this case, the sample was stirred with a magnetic stirrer. The pH sorption edge was carried out in the pH range 3 to 7. Once prepared, solutions were shaken in an oscillating table for 24 hours after which the final pH meter reading was taken.

REE, Sc, Y, Th and U concentrations in solution were measured using a Quadrupole ICP-MS (Agilent Technologies 7700x). The concentrations were determined using a conventional external calibration procedure with multi-elemental solutions, acidified to 2% in nitric acid ( $\text{HNO}_3$ ), from 0.005 to 2  $\mu\text{g L}^{-1}$ . Rhodium solution was used as an internal standard to correct the instrumental drift. The international geostandard SLRS-6 was used to check the validity and reproducibility of the results. Collision cell technology with helium ( $\text{He}$ ) gas, was used to limit or eliminate potential interferences (Yeghicheyan et al., 2019). Typical uncertainties including all error sources were below  $\pm 5\%$  for all the trace elements. The limit of detection and the isobaric interferences for all the groups of metal ions were calculated following the procedure at Rennes previously mentioned in Davranche et al., (2004).

Percentage of metal ion adsorbed ( $\%M_{\text{ads}}$ ) and distribution coefficient ( $K_d, \text{L kg}^{-1}$ ) were used to express the metal ion adsorption onto quartz surface:

$$\%M_{\text{ads}} = \frac{[M]_{\text{tot}} - [M]_{\text{aq}}}{[M]_{\text{tot}}} \times 100 \quad (1)$$

$$K_d = \frac{[M]_{tot} - [M]_{aq}}{\frac{m}{V} \times [M]_{aq}} \quad (2)$$

where  $[M]_{tot}$  and  $[M]_{aq}$  refer to the total (initial) metal ion concentration and its concentration in solution after phase separation, respectively, and  $m/V$  is the solid to liquid ratio expressed as mass of a solid (in kg) in contact with a solution of a given volume (in L). Several physico-chemical conditions may affect the  $K_d$  values such as pH, ionic strength, temperature, etc.

### 2.3 Column experiments

The sorption of REE onto quartz under flow through conditions was investigated using a liquid chromatography system (Äkta™ Pure) equipped with a fraction collector (F9-R). Previously cleaned 15 g of Fontainebleau quartz sand was dry-packed in a borosilicate column (XK 16, GE Healthcare) with an internal diameter of 1.6 cm. The porous bed height was approximately 5 cm with a uniform bulk density of  $1.65 \text{ g cm}^{-3}$ . The column was wetted upward with 5 mM NaCl solution at a pH of 5 at a flow rate of  $0.1 \text{ mL min}^{-1}$ , which corresponds to a flow velocity of  $0.05 \text{ cm min}^{-1}$ . Once the column was fully saturated, a tracer test was performed with potassium bromide (KBr solution) (Figure S1) to identify the flow characteristics which was described by the advection dispersion equation (ADE). KBr was injected at a constant flow rate in a pulse mode; 2 mL of tracer solution followed by background electrolyte solution. The homogeneous flow and the predominantly convective regime were confirmed after analysing the breakthrough curve (BTC) using inverse modeling with HYDRUS 1D (Šimůnek et al., 2013).

For the reactive transport, aqueous REY, Sc, Th and U, solutions containing  $5 \mu\text{g L}^{-1}$  of each metal ( $C_0$ ), corresponding to  $7 \times 10^{-7} \text{ M}$  of the total metal ion concentration, with 5 mM NaCl at pH 5 were injected in the column at a flow rate of 0.1 or  $1 \text{ mL min}^{-1}$ . Samples of the outflow solution were collected by volume of 5 mL in tubes of 18 mm diameter with the fraction collector and the aqueous metal ions concentrations ( $C$ ) were measured using ICP-MS. This allowed to calculate the relative concentration ( $C/C_0$ ) of each metal ion in the outflow solutions.

### 2.4 Surface Complexation and Reactive Transport Modeling

Surface complexation on quartz was modeled using PHREEQC version 2 (Parkhurst and Appelo, 1999). The thermodynamic database “Minteq v4” was used. This database has been updated by incorporating well-accepted stability constants at 0 M ionic strength and  $25 \text{ }^\circ\text{C}$  for REY inorganic anion complexation relevant to the present work including: (i) chloride ( $\text{REYCl}_2^+$ ,  $\text{REYCl}^+$ ) (Luo and Byrne, 2001) (ii) hydroxide ( $\text{REYOH}^{2+}$ ,  $\text{REY(OH)}_2^+$ ,  $\text{REY(OH)}_3$ ) (Klungness and Byrne, 2000), (iii) bicarbonate and carbonate ( $\text{REYHCO}_3^{2+}$ ,  $\text{REYCO}_3^+$  and  $\text{REY(CO}_3)_2^-$ ) (Luo and Byrne, 2004). Th and U database is taken from Nuclear Energy Agency (NEA) (Guillaumont et al., 2003). Sc hydrolysis constants are taken from Brown and Ekberg, (2016). The reactions and the constant database for REY and Sc is provided in Appendix (Table S1). Note that  $\text{REY(OH)}_{3(s)}$  precipitation along with  $\text{Sc(OH)}_{3(s)}$ , Schoepite and  $\text{Th(OH)}_{4(s)}$  did not occur in our experiments according to the model.

The surface complexation model in this study was derived from the model of García et al. (2019). In this model, two types of sites are considered: first type of sites (site x) shows an amphoteric behaviour

whereas the second type of sites (site  $y$ ) only undergoes deprotonation. The total site density of  $x$  and  $y$  sites equals  $1 \text{ nm}^{-2}$  and  $3.7 \text{ nm}^{-2}$ , respectively (Hiemstra et al., 1989; García et al., 2019). All concerning information are given in Table 1. Surface species concentrations are expressed with a mole fraction scale in PHREEQC (Parkhurst and Appelo, 1999; Lützenkirchen et al., 2015). A Basic Stern Model (BSM) is used to define interfacial electrostatics of the system, with a capacitance of  $2 \text{ F m}^{-2}$ . The charge of  $\text{H}^+$  ions is placed at the surface (0-plane) whereas for  $\text{Cl}^-$  and  $\text{Na}^+$  the charge is located at the 1-plane. The charge of REY, Sc, Th and U ions was distributed at the quartz/water interface between 0-plane and 1-plane, as they form innersphere complexes with metal oxide surfaces (Dzombak and Morel, 1990; Rabung et al., 1998; Schnurr et al., 2015; Wu et al., 2020). Outersphere complexation of these ions occurs in the diffuse double layer, but this process appeared negligible compared to innersphere surface complexation one. PhreePlot was used to estimate parameters for metal ions adsorption to quartz (Kinniburgh and Cooper, 2009). Using a modified Marquardt–Levenberg procedure (Powell, 1965), PhreePlot provides a statistical uncertainty for the estimated parameters, which are reported in this study. The surface area of the quartz particles could not be measured as it is very small, but was found equal to  $0.07 \text{ m}^2 \text{ g}^{-1}$  with Phreeplot, which is close to  $0.05 \text{ m}^2 \text{ g}^{-1}$  estimated from geometrical consideration.

Surface complexation reactions at equilibrium were coupled with advection dispersion equation (equation (3)) in PHREEQC to simulate the breakthrough curves of the REY, Sc, Th and U in column. The aqueous concentrations of the metal ions are governed by the following advection-reaction-dispersion (ARD) equation (Parkhurst and Appelo, 1999)

$$\frac{\partial C}{\partial t} = -v \frac{\partial C}{\partial x} + D_L \frac{\partial^2 C}{\partial x^2} - \frac{\partial q}{\partial t} \quad (3)$$

where  $C$  is the concentration in water ( $\text{kg m}^{-3}$ ),  $t$  is time (s),  $v$  is pore water flow velocity ( $\text{m s}^{-1}$ ),  $x$  is distance (m),  $D_L$  is the hydrodynamic dispersion coefficient ( $\text{m}^2 \text{ s}^{-1}$ ), and  $q$  is concentration in the solid phase (expressed as  $\text{kg m}^{-3}$  in the pores). The numerical approach in PHREEQC follows the basic components of ARD equation in a split-operator scheme (Parkhurst and Appelo, 1999). First, advective transport was calculated, followed by calculation of equilibrium controlled chemical reactions, and dispersive transport. The chemical interaction term  $\frac{\partial q}{\partial t}$  calculated separately from the transport part for each time step is the sum of all equilibrium reaction rates.

**Table 1.** Model parameters: protolysis reaction and reaction of background electrolyte onto quartz surface with a BSM (capacitance equal to 2 F m<sup>-2</sup>). Surface site densities are 1 (site x) and 3.7 nm<sup>-2</sup> (site y). Surface area is equal to 0.07 m<sup>2</sup> g<sup>-1</sup>. Present study revealed that y-type sites must be divided into strong and weak sites with densities of 0.135 and 3.565 nm<sup>-2</sup>, respectively (see section 3.3).

Surface reaction	Log K	$\Delta z_0$	$\Delta z_1$
$Si_xOH + H^+ \rightleftharpoons Si_xOH_2^+$	- 1.3	+1	0
$Si_xOH \rightleftharpoons Si_xO^- + H^+$	- 4.0	-1	0
$Si_xO^- + Na^+ \rightleftharpoons Si_xONa$	1.9	0	+1
$Si_xOH_2^+ + Cl^- \rightleftharpoons Si_xOH_2Cl$	5.4	0	+1
$Si_yOH \rightleftharpoons Si_yO^- + H^+$	- 8.5	-1	0
$Si_yO^- + Na^+ \rightleftharpoons Si_yONa$	1.5	0	-1

### 3 Results and discussion

#### 3.1 Adsorption of REY, Sc, Th and U onto quartz sand

Adsorption kinetics data showed that an equilibrium was reached within less than 8 hours (as illustrated for Eu in Figure S2), and that adsorption kinetics followed a pseudo-second order model as shown in the following equation:

$$q_t = \frac{k_2 q_e^2 t}{k_2 q_e t + 1} \quad (4)$$

where  $t$  is time (min),  $q_t$  is the amount of adsorbed solute at time  $t$  ( $\mu\text{g g}_{\text{sand}}^{-1}$ ),  $q_e$  is its value at equilibrium ( $\mu\text{g g}_{\text{sand}}^{-1}$ ) and  $k_2$  is the pseudo-second order rate constant ( $\text{g}_{\text{sand}} \mu\text{g}^{-1} \text{min}^{-1}$ ). The value for  $k_2$  determined for Eu (in the presence of the other REY, Sc, Th and U) by using a least-square fit approach was found to (i) increase with pH at high loading ( $[M] = 7 \times 10^{-7} \text{ M}$ ), from 0.561 (pH = 5.5) to 0.612 (pH = 6.5)  $\text{g}_{\text{sand}} \mu\text{g}^{-1} \text{min}^{-1}$ , (ii) increase with decreasing loading at pH = 5.5, as it reached 0.944  $\text{g}_{\text{sand}} \mu\text{g}^{-1} \text{min}^{-1}$  for  $[M] = 10^{-7} \text{ M}$ . This showed that the rate and the extent of metal ion uptake can be influenced by both pH and initial metal ion concentration.

The adsorption of Eu onto quartz versus pH in the presence of the other REY, Sc, Th and U in 5 mM NaCl solution is shown in Figure 1a,b for the total metal ion concentrations of  $7 \times 10^{-7} \text{ M}$  and  $10^{-7} \text{ M}$ , respectively. Adsorption data for some selected REE (La, Ho and Lu) are also shown for comparison in Appendix (Figure S3). As typically encountered for cations adsorption onto quartz and metal oxides, REE binding to quartz surface increased with pH (Dzombak and Morel, 1990; Stumm and Morgan, 1996; Rabung et al., 1998; Naveau et al., 2005; García et al., 2019). This is due to the intrinsic chemical affinity of REE to quartz surface sites and the electrostatic attraction between negatively charged quartz surface and positively charged metal ions (Jajala et al., 2006; García et al., 2019). For the high metal ion concentrations ( $7 \times 10^{-7} \text{ M}$ , Figure 1a), the adsorption started at around pH 4 and reaches almost 95% at pH 7. In addition, the pH-edge envelop did not have a simple sigmoid shape: the adsorption follows two stages, hence suggesting the occurrence of two distinct adsorption processes. These results are in excellent agreement with previous studies (García et al., 2019), where the formation of two surface species were identified at low and high pH involving different stoichiometric coefficients for the proton. However, the present results show that the pH-edge envelop is concentration dependent, because the adsorption increases more steeply with pH at low metal ion concentrations ( $10^{-7} \text{ M}$ , Figure 1b) than for higher ones ( $7 \times 10^{-7} \text{ M}$ , Figure 1a). This suggests involvement of a certain amount of high affinity sites at the quartz surface, as previously observed for metal ions adsorption onto, for instance, hydrous ferric oxides (Dzombak and Morel, 1990), hematite (Rabung et al., 1998), clays (Schnurr et al., 2015) and goethite (Wu et al., 2020).

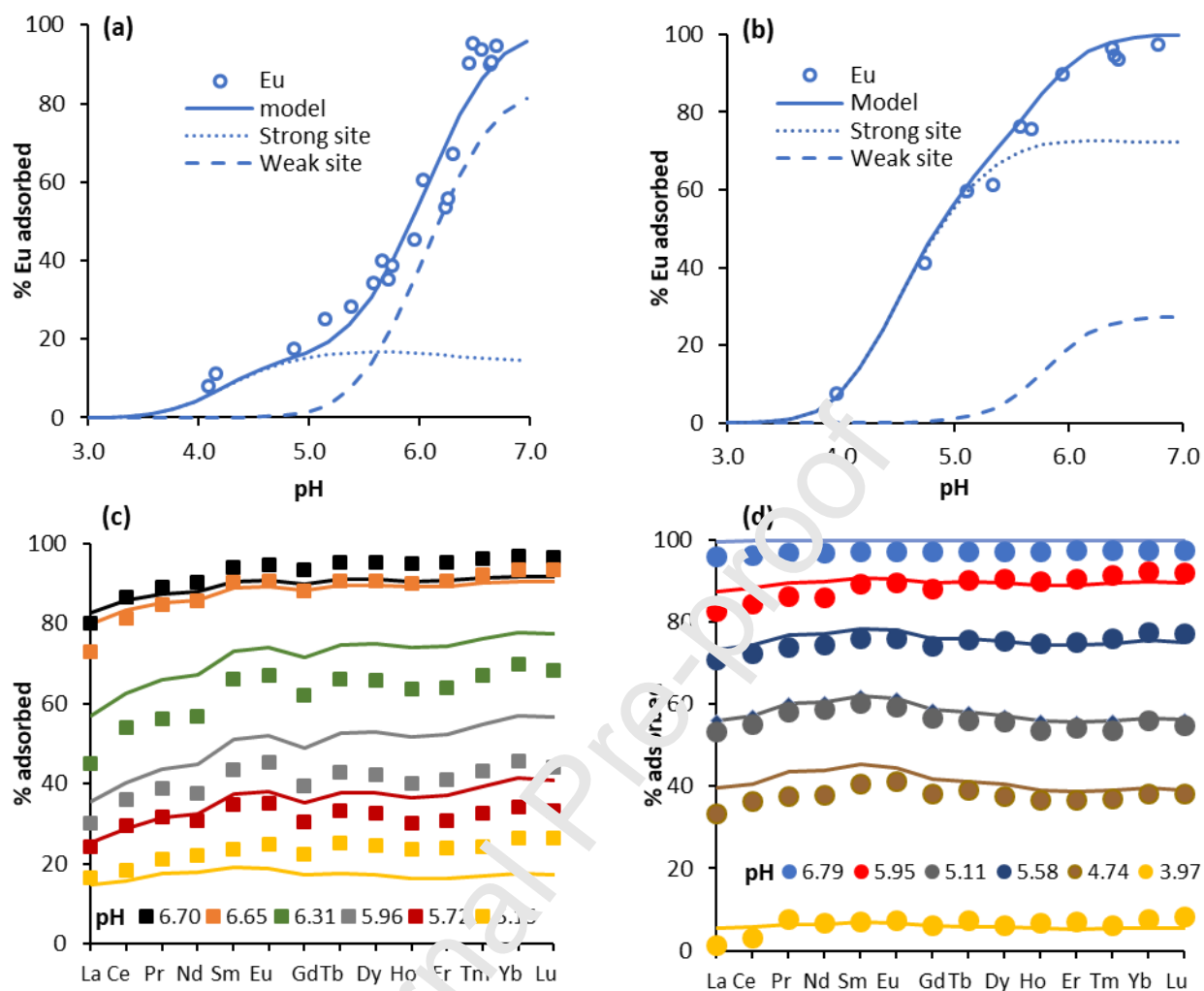


**Figure 1.** Experimental and modeled Eu adsorption data onto quartz as a function of pH for total metal ions concentration of (a)  $7 \times 10^{-7}$  M and (b)  $10^{-7}$  M. Corresponding percentage of REE adsorbed as a function of atomic number ("REE patterns") at different pH values for total metal ions concentration of (c)  $7 \times 10^{-7}$  M (d)  $10^{-7}$  M. REE patterns are shown in Figure S4. Experimental data are represented by markers, whereas the solid lines represent the surface complexation model results.

The REE patterns obtained at different pH values are plotted as percentage adsorbed against the atomic number in Figure 1c,d, for  $7 \times 10^{-7}$  M and  $10^{-7}$  M, respectively. A M-type tetrad effect can be observed which shows that REE adsorbed predominantly by inner-sphere complexation (Takahashi et al., 2000, 2005). For high REE concentrations at low pH, middle REE (MREE) are preferentially adsorbed over light REE (LREE) and heavy REE (HREE) (see Figure 1c, pH 5.15). However, REE pattern evolved at pH > 6, where HREE are preferentially adsorbed over LREE and MREE. One possible reason for this variation in the REE pattern could be the occurrence of a second type of surface complex that is prevalent at high metal ion

surface loadings and high pH values. Therefore, the surface complexation model should account for this shift in the REE pattern likely arising from two distinct adsorption mechanisms. At low REE loading (see Figure 1d), a single pattern increasing for MREE was observed for the whole investigated pH range. This is in line with the hypothesis of the prevalence of a single type of REE surface complex at low surface loadings. The occurrence of two surface complexation processes, corresponding to high affinity and low affinity sites, may alter REE adsorption patterns, as previously observed for heterogeneous adsorbent such as natural organic matter (NOM), nanoplastics or bacterial cells (Takahashi et al., 2005, 2010; Marsac et al., 2010, 2011, 2021; Catrouillet et al., 2019; Blancho et al., 2022). For NOM, REE patterns have been successfully applied to describe preferential adsorption of REE onto carboxylic and phenolics or chelate binding sites, respectively (Marsac et al., 2010; 2011), which was affected by competition with other cations such as  $\text{Al}^{3+}$  or  $\text{Fe}^{3+}$  (Marsac et al., 2012; 2013; 2021). In case of REE adsorption to nanoplastics, REE patterns were shown to differentiate between low affinity mono-dentate complexation sites and high affinity bi-dentate complexation sites (Blancho et al., 2022). Similarly, on the bacterial cell walls, or organic matter of bacterial origin, REE patterns evidenced two different types of binding mechanisms to carboxylate and phosphate groups (Takahashi et al., 2005, 2010; Catrouillet et al., 2019). Therefore, REE patterns can be considered as important tools to highlight the presence of various binding sites at the surface of natural adsorbents.

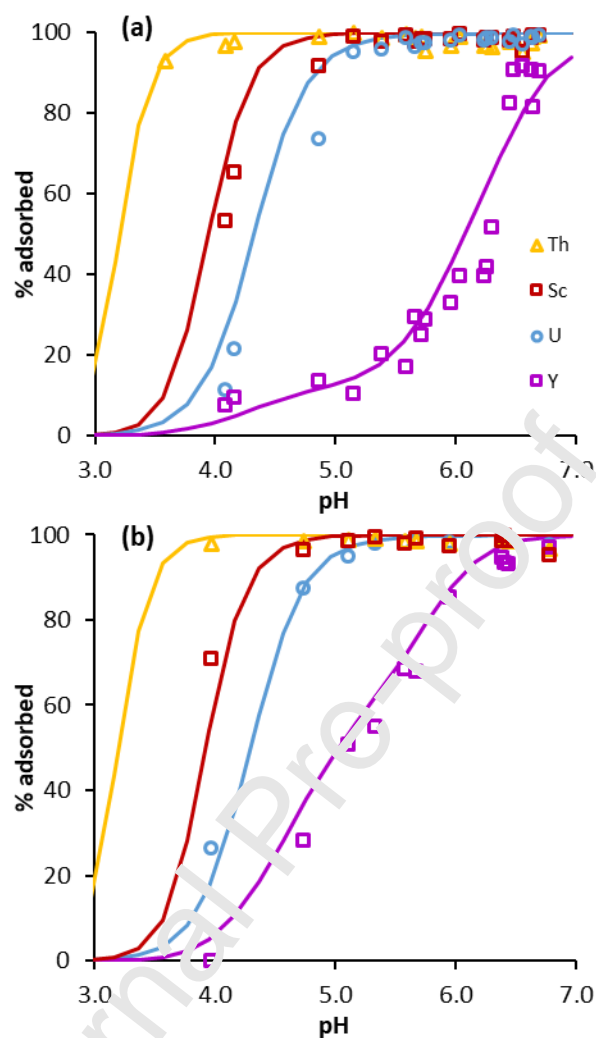


**Figure 2.** Percentage adsorbed for Sc, Y, Th and U onto quartz for total metal ion concentration of (a)  $7 \times 10^{-7}$  M and (b)  $10^{-7}$  M.

Adsorption of REE was compared with the adsorption of Sc, Y, Th and U. The pH-edge envelop of Y (Figure 2) showed a concentration dependence similar to REE, as evidenced by steeper adsorption increase with pH at low metal concentration than at high metal concentration possibly due to the presence of two distinct sites. This is consistent with the geochemically similar behavior of Y and Ho (one of the REE) due to similar charge and ionic radii (1.019 Å for  $Y^{3+}$  and 1.015 Å for  $Ho^{3+}$ , both with a coordination number (CN) of 8) (Shannon, 1976). By contrast, Scandium showed stronger adsorption compared to REE. At pH  $\sim$  4, the percentage of Sc adsorbed was 70 % and 50 % for low and high metal concentrations, respectively (Figure 2). This can be explained by the smaller ionic radius of  $Sc^{3+}$ : 0.87 Å for CN = 8, which is a considerably lower value than  $Lu^{3+}$ , the smallest lanthanide (0.98 Å with CN 8). Th occurs as a tetravalent cation resulting in its strong surface complexation onto minerals including quartz (Reiller et al., 2003; Geckeis et al., 2013). Finally, in aqueous solutions U (VI) is generally prevalent, however under reducing conditions U (IV) can also exist (Fletcher et al., 2010). As the experiments were conducted under oxidizing conditions U mainly exist as a uranyl ion ( $UO_2^{2+}$ ) in aqueous solutions, and

behaves as a cation with an effective charge of +3.3 (Choppin and Rao, 1984; Geckeis et al., 2013), which may explain why its adsorption is generally stronger than that of REE. The present results for U are also in agreement with previous studies (e.g. (Turner and Sassman, 1996; Prikryl et al., 2001; Davis et al., 2004; Nair et al., 2014; Zavarin et al., 2022)). Unlike REY, the pH adsorption edges of Sc, Th and U was unaffected by metal loading within the present range of experimental conditions. This can be explained by either (i) a preferential binding of these cations to the strong surface sites or (ii) similar binding affinities for both weak and strong sites.

Journal Pre-proof

### 3.2 Transport of REE in sand columns

To assess the potential mobility of aqueous REY, Sc, Th and U, solutions containing  $5 \mu\text{g L}^{-1}$  of each metal were injected through fixed-bed columns packed with quartz sand particles. The breakthrough curves (BTCs) shown in Figure 3a for La, Eu and Lu, chosen as examples of LREE, MREE and HREE respectively, show that REE did not break out before the injection of 40 pore volumes (PV). This delayed breakthrough indicated that REE were strongly retained in the quartz sand column under flow-through conditions. The total adsorbed amounts at complete breakthrough (La  $\sim 0.007 \mu\text{mol m}^{-2}$ , Eu  $\sim 0.008 \mu\text{mol m}^{-2}$  and Lu  $\sim 0.005 \mu\text{mol m}^{-2}$ ) were in close agreement with those expected from the batch sorption data. Stronger adsorption of MREE in the column pushed the breakthrough point of Eu up to 47 PV compared to 43 PV for La and Lu. Two distinct shapes in the BTC of REE were observed depending on the REE type. For instance, La and Lu showed similar BTCs, while that of Eu exhibited a long tailing before a complete breakthrough (i.e.  $C/C_0 = 1$ ) occurring at 113 PV. The relative concentration for La and Lu exceeded 1 after their complete breakthrough at 59 PV, before decreasing back to  $C/C_0 = 1$  at around 80 PV. This may result from a release of previously adsorbed LREE and HREE, thereby suggesting preferential adsorption of MREE, Sc, Th and U, onto the quartz surface. This competitive adsorption may also explain the extended tailing observed in the BTC of Eu, where Eu continued to adsorb and compete with La and Lu for the surface sites of quartz. This could also be confirmed by the REE patterns in the column effluent normalized to the inlet concentration (Figure 3b). Indeed, the REE patterns showed MREE depletion with respect to LREE and HREE indicating higher retention of MREE and higher mobility of LREE and HREE in the column. This pattern was similar to the inverted REE patterns obtained under batch conditions at low REE concentration (see Figure 1d). In fact, surface loadings in column were comparable to batch data at low metal concentrations ( $0.15 \mu\text{mol m}^{-2}$  for column vs.  $0.12 \mu\text{mol m}^{-2}$  for batch) (Figure S5). Hence, the same type of REE surface complexes could be expected in both systems, which was characteristic of low metal loading under batch conditions.

The transport behaviour of Y was very similar to that of the LREE or HREE, with the breakthrough point at 43 PV and the complete breakthrough occurring at 59 PV. Similar to the batch results, the adsorption of U in the column was stronger than REY delaying the breakthrough until 56 PV. However, the complete breakthrough was not achieved within the experimental timescale. For Th and Sc, the adsorption was very strong in the dynamic column experiment and thus no breakthrough was observed.

To check whether kinetic limitations took place under flow conditions, a ten-fold increase in the flow rate ( $\sim 1 \text{ mL min}^{-1}$ ) was tested (Figure S6). No significant change in the breakthrough point was observed for all metals except for U (earlier breakthrough point). However, the BTCs of La, Eu and Lu showed an extended tailing at higher flow rate, and no desorption of previously adsorbed elements has been noted (i.e.  $C/C_0 > 1$ ).

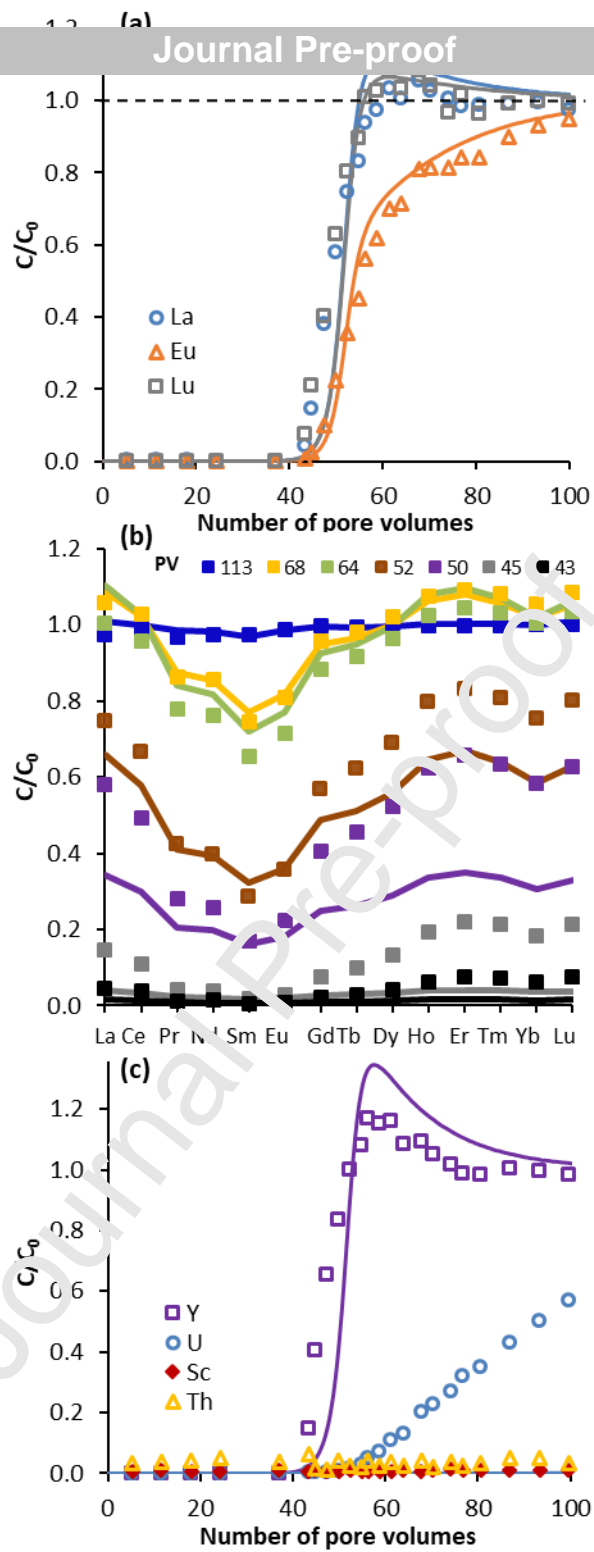
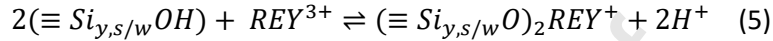


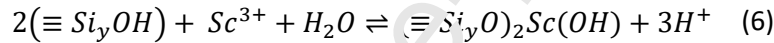
**Figure 3.** (a) Experimental and modeling breakthrough curves for La, Eu and Lu. (b) REE patterns in the column for different PV injected. (c) Experimental and modeling breakthrough curves for Sc, Y, Th and U.

### 3.3 Surface complexation and reactive transport modeling

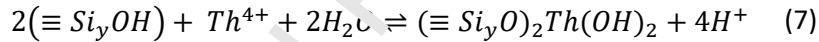
According to García et al. (2019), quartz surface exhibits two types of sites ( $x$  and  $y$ ) but only cation binding to  $y$  sites is considered. Present experimental results evidenced two distinct adsorption mechanisms, suggesting that  $y$ -type sites must be divided into 2 subsets of high affinity and low affinity sites, with identical reaction and constants with protons and background electrolytes (Table 1). At low metal loading, REY formed a surface complex on the high affinity (or strong, “s”) sites ( $\equiv Si_{y,s}OH$ ) which was more prevalent at low pH values (Table 2). At higher metal loading, REY formed a complex involving low affinity (or weak, “w”) sites ( $\equiv Si_{y,w}OH$ ). Both of these inner-sphere surface complexation reactions could be expressed by the following generic reaction:



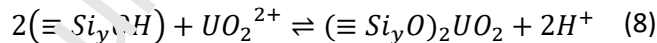
The surface complexation reaction differed from that of García et al., (2019), where two surface species involving different stoichiometries for  $H^+$  were used. This is due to the fact that strong and weak sites were considered in the present work, contrary to García et al., (2019) where the two surface complexation processes had to be distinguished by different reactions. For Sc, surface complexation reaction involving a hydrolysed surface species was considered:



The adsorption of Th was assumed to involve the same hydrolysis expressed as:



This did not exclude the formation of less hydrolysed Sc or Th surface species, but they might prevail at lower pH values than those presently investigated. Finally, to account for the U(VI) adsorption onto quartz a single reaction was used, similarly to that of REY:



To decrease the number of adjustable parameters, it was assumed that the REE pattern of the surface complexation constants with strong and weak sites had the same shape as the patterns recorded in column and in batch at high surface loading, respectively. Column REE pattern ( $C/C_0$ ) at pore volume 52 (denoted  $C/C_{0,PV=52}$ ) and  $\log K_d$  pattern at pH = 6.7 and  $[M] = 7 \times 10^{-7}$  M (denoted  $K_{d,high}$ ) were respectively selected for that purpose:

$$\log K_{s,REE} = a \times C/C_{0,PV=52} + b \quad (9)$$

$$\log K_{w,REE} = c \times \log K_{d,high} + d \quad (10)$$

Where  $a$ ,  $b$ ,  $c$  and  $d$  are adjustable parameters of the linear relationships ( $a = -0.22 \pm 0.06$ ,  $b = -2.63 \pm 0.11$ ,  $c = 0.72 \pm 0.06$ ,  $d = -9.12 \pm 0.25$ ). The  $\log K$  values for Sc, Y, Th and U along were fitted individually. For Sc, Th and U, the present experimental dataset did not allow us to include high affinity and low affinity sites. Therefore, same surface complexation constant values were assumed at both sites. Final site densities were found equal to  $0.135 \text{ nm}^{-2}$  and  $3.565 \text{ nm}^{-2}$  for strong and weak  $y$ -type sites,

respectively. For reactions concerning REY, the charge variation at the 0- and 1-planes ( $\Delta z_0$ ;  $\Delta z_1$ ) was determined together with the surface complexation constants during the fit with Phreeplot. The charge variation of Sc at 1-plane was constrained based on the  $\Delta z_1$  value of the REY with an addition of -1 charge to account for the charge of hydroxide ion. The same reasoning was applied for Th where -2 charges are placed at the 1-plane. For U,  $\Delta z_0$  value was set equal to that of the REY.

Results of the fit with Phreeplot are shown in Figures 1 and 2. Overall the model predicted relatively well the effects of pH and surface loading on the adsorption on each of the studied cations and, hence, of REE adsorption patterns. Simulations of the surface speciation revealed that, at low metal loading (Figure 1b), REY adsorption processes were controlled mainly by the few strong sites at pH < 5.7. Above this pH value, the strong sites became saturated and competition between weak and strong sites occurred. At higher metal concentrations (Figure 1a), REE adsorption occurred at the strong sites at low pH values, until strong sites are saturated. When pH increased, the adsorption of REE was controlled by the weak sites. This shift from the strong to weak sites with pH corresponding to two distinct adsorption mechanisms was evidenced by the change in the slope of the pH adsorption edge at pH  $\approx$  5.7. The corresponding change in the REE pattern from MREE preferential adsorption at strong sites to HREE preferential adsorption at weak sites was also well captured (Figure 1c,d). Because the same binding constants were assumed for strong and weak sites for Sc, Th and U, only one type of surface species could explain the whole adsorption behaviour. The multi-element REE SCM developed in this study also predicted relatively well literature data of Eu sorption onto quartz García et al. (2019) (Figure S7), when accounting for the effects of high ionic strength with the Pitzer equation (included e.g. in the THEREDA database (Moog et al., 2015)).

Using the batch-derived surface complexation parameters (see Table 2) and the hydrodynamic parameters defined by the tracer breakthrough, the reactive transport model developed in PHREEQC could well describe the experimental BTCs (see Figure 3a). Only a slight adjustment of the surface complexation constant was made, by reducing the log K of all REY values by 0.5, which is close to the range of uncertainty. The 1-D transport model captured many of the observed features, namely: (i) the breakthrough points for REY, (ii) the extended tailing for MREE, and (iii) the desorption of LREE and HREE induced by competition with MREE resulting in  $C/C_0 > 1$ . The model, however, overestimated the sorption of U in the column as no breakthrough was observed in the model. This might be due to kinetic limitations that may cause earlier breakthrough for U. Indeed, varying flow rates or residence times in the column have influenced the BTC of U, yet no significant change in mobility behaviour was observed for the other metals.

Overall, the model was able to predict correctly the strong adsorption behaviour for Sc and Th in the column. The REE pattern predicted by the transport modeling (Figure 3b) fitted well the experimental data, confirming that MREE are preferentially adsorbed. This study demonstrated that transport modeling using hydrodynamic parameters defined by the tracer breakthrough experiment and the surface complexation reactions involving strong and weak sites could be successfully used to predict not only the mobility of REE through quartz, but also the competition between different REE for surface sites.

Journal Pre-proof

**Table 2.** Surface complexation model parameters for REE and Sc, Y, Th and U sorption onto Fontainebleau quartz sand.

Surface species	Log K of the weak sites	Log K of the strong sites	$\Delta z_0$	$\Delta z_1$
$(\equiv Si_yO)_2La^+$	$-7.25 \pm 0.40$	$-2.79 \pm 0.22$		
$(\equiv Si_yO)_2Ce^+$	$-7.10 \pm 0.41$	$-2.78 \pm 0.22$		
$(\equiv Si_yO)_2Pr^+$	$-7.03 \pm 0.41$	$-2.72 \pm 0.23$		
$(\equiv Si_yO)_2Nd^+$	$-6.99 \pm 0.42$	$-2.72 \pm 0.23$		
$(\equiv Si_yO)_2Sm^+$	$-6.83 \pm 0.43$	$-2.69 \pm 0.23$		
$(\equiv Si_yO)_2Eu^+$	$-6.79 \pm 0.43$	$-2.71 \pm 0.23$		
$(\equiv Si_yO)_2Gd^+$	$-6.85 \pm 0.43$	$-2.75 \pm 0.23$		
$(\equiv Si_yO)_2Tb^+$	$-6.76 \pm 0.44$	$-2.77 \pm 0.23$	$-0.2 \pm 0.1$	$1.2 \pm 0.1$
$(\equiv Si_yO)_2Dy^+$	$-6.74 \pm 0.44$	$-2.78 \pm 0.23$		
$(\equiv Si_yO)_2Ho^+$	$-6.76 \pm 0.44$	$-2.81 \pm 0.22$		
$(\equiv Si_yO)_2Er^+$	$-6.75 \pm 0.44$	$-2.81 \pm 0.22$		
$(\equiv Si_yO)_2Tm^+$	$-6.68 \pm 0.44$	$-2.81 \pm 0.22$		
$(\equiv Si_yO)_2Yb^+$	$-6.63 \pm 0.45$	$-2.80 \pm 0.23$		
$(\equiv Si_yO)_2Lu^+$	$-6.64 \pm 0.45$	$-2.81 \pm 0.22$		
$(\equiv Si_yO)_2Y^+$	$-6.99 \pm 0.42$	$-2.85 \pm 0.22$		
$(\equiv Si_yO)_2Sc(OH)$	$-6.01 \pm 0.07$	$-6.01 \pm 0.07$	$-0.2 \pm 0.1$	$0.2 \pm 0.1$
$(\equiv Si_yO)_2Th(OH)_2$	$-5.37 \pm 0.39$	$-6.37 \pm 0.39$	$0.8 \pm 0.1$	$-0.8 \pm 0.1$
$(\equiv Si_yO)_2UO_2$	$-3.18 \pm 0.09$	$-3.18 \pm 0.09$	$-0.2 \pm 0.1$	$0.2 \pm 0.1$

## 4 Conclusions

Here, we have investigated the interactions of REE, Y, Sc, Th and U with the most abundant mineral in the environment, quartz, under both batch and dynamic flow conditions. Our work notably uncovered several important and unforeseen processes that might play an important role on the fate and behaviour of REE in environmental systems. Despite its low specific surface area, quartz sand particles were shown here to strongly bind REE along with Y, Sc, Th and U, and thus alter their transport and mobility under flow-through conditions. In addition, two types of binding surface sites with different densities were found to control metal ions adsorption to quartz: (i) less abundant high affinity sites preferentially bind middle REE at lower REE loading and (ii) more abundant low affinity sites preferentially bind heavy REE at higher REE loading. This further illustrates the great utility of REE pattern as an efficient probe of surface complexation processes at heterogeneous mineral surfaces. Considerable competition effects were also observed between metal ions for the strong sites because of their relatively small surface density. This was particularly important under flow through conditions, where the more strongly binding MREE, Sc, Th and U ions moved to the REE and Y out of the column, which lead to larger concentrations of these latter ions in the outflow solution ( $C/C_0 > 1$ ). A mechanistic surface complexation model was developed to account for the occurrence of strong and weak surface sites, which allowed accurate predictions of REE, Sc, Y, Th and U adsorption to quartz versus pH and metal ion concentration. Reactive transport model assuming a local equilibrium and using batch-derived parameters could capture relatively well the transport behaviour of REE, including competitive effects between metal ions. All these results highlight the need of an accurate description of complexation reactions of REE at environmental surfaces. In addition, the presently investigated reactive transport model might pave the way for the development of new powerful tools for the prediction of the fate and transport of REE in natural systems. However, because natural systems are characterized by a large heterogeneity, further experimental and modeling investigations of REE interactions with various minerals under varying solution chemistry (e.g. presence of dissolved anions or natural organic matter) are required.

## 5 Acknowledgements

This project has received funding from the European Union's Horizon 2020 research and innovation programme under the Marie Skłodowska-Curie Grant Agreement N° 857989 (PANORAMA project). Through the support of the GeOHeLiS analytical platform of Rennes University, this publication is also supported by the European Union through the European Regional Development Fund (FEDER), the French Ministry of Higher Education and Research, the French Region of Brittany and Rennes Metropole. The authors are grateful to M. Bouhnik-Le Coz for the assistance in ICP-MS analysis.

## 6 References

- Altmaier M., Gaona X. and Fanghänel T. (2013) Recent Advances in Aqueous Actinide Chemistry and Thermodynamics. *Chem. Rev.* **113**, 901–943.
- Amiel N., Dror I. and Berkowitz B. (2022) Mobility and Retention of Rare Earth Elements in Porous Media. *ACS Omega* **7**, 19491–19501.
- Anastopoulos I., Bhatnagar A. and Lima E. C. (2016) Adsorption of rare earth metals: A review of recent literature. *Journal of Molecular Liquids* **221**, 954–962.
- Balaram V. (2019) Rare earth elements: A review of applications, occurrence, exploration, analysis, recycling, and environmental impact. *Geoscience Frontiers* **10**, 1285–1303.
- Bau M. (1999) Scavenging of dissolved yttrium and rare earths by precipitating iron oxyhydroxide: experimental evidence for Ce oxidation, Y-Ho fractionation and Lanthanide tetrad effect. *Geochimica et Cosmochimica Acta* **63**, 67–77.
- Blanco F., Davranche M., Marsac R., Léon A., Dia A., Grassl S., Reynaud S. and Gigault J. (2022) Metal-binding processes on nanoplastics: rare earth elements as probes. *Environmental Science: Nano* **9**, 2094–2103.
- Brown P. L. and Ekberg C. (2016) *Hydrolysis of metal ions*, John Wiley & Sons.
- Bryan N. D., Barlow J., Warwick P., Stephens S., Higgs J. J. W. and Griffin D. (2005) The simultaneous modelling of metal ion and humic substance transport in column experiments. *J. Environ. Monit.* **7**, 196–202.
- Catrouillet C., Guenet H., Pierson-Wickmann A.-C., Dia A., LeCoz M. B., Deville S., Lenne Q., Suko Y. and Davranche M. (2019) Rare earth elements as tracers of active colloidal organic matter composition. *Environ. Chem.* **17**, 133–139.
- Cheng W., Kalahroodi E. L., Marsac R. and Hanna K. (2019) Adsorption of Quinolone Antibiotics to Goethite under Seawater Conditions: Application of a Surface Complexation Model. *Environ. Sci. Technol.* **53**, 1130–1138.
- Choppin G. R. and Rao L. F. (1984) Complexation of Pentavalent and Hexavalent Actinides by Fluoride. *Radiochimica Acta* **37**, 143–146.
- Davis J. A., Meece D. E., Kohler M. and Curtis G. P. (2004) Approaches to surface complexation modeling of Uranium(VI) adsorption on aquifer sediments. Associate editor: J. Rustad. *Geochimica et Cosmochimica Acta* **68**, 3621–3641.
- Davranche M., Pourret O., Gruau G. and Dia A. (2004) Impact of humate complexation on the adsorption of REE onto Fe oxyhydroxide. *Journal of Colloid and Interface Science* **277**, 271–279.
- Davranche M., Pourret O., Gruau G., Dia A. and Le Coz-Bouhnik M. (2005) Adsorption of REE(III)-humate complexes onto MnO<sub>2</sub>: Experimental evidence for cerium anomaly and lanthanide tetrad effect suppression. *Geochimica et Cosmochimica Acta* **69**, 4825–4835.

- Drobniak A. and Mastalerz M. (2022) Rare Earth Elements: A brief overview. *Indiana Journal of Earth Sciences* **4**.
- Dzombak D. A. and Morel F. M. (1990) *Surface complexation modeling: hydrous ferric oxide.*, John Wiley & Sons.
- Fairhurst A. J., Warwick P. and Richardson S. (1995) The Effect of pH on Europium-Mineral Interactions in the Presence of Humic Acid. *Radiochimica Acta* **69**, 103–112.
- Fletcher K. E., Boyanov M. I., Thomas S. H., Wu Q., Kemner K. M. and Löffler F. E. (2010) U(VI) Reduction to Mononuclear U(IV) by Desulfitobacterium Species. *Environ. Sci. Technol.* **44**, 4705–4709.
- García D., Lützenkirchen J., Petrov V., Siebentritt M., Schild D., Lefèvre G., Rabung T., Altmaier M., Kalmykov S., Duro L. and Geckeis H. (2019) Sorption of Eu(III) on quartz at high salt concentrations. *Colloids and Surfaces A: Physicochemical and Engineering Aspects* **578**, 123610.
- Geckeis H., Lützenkirchen J., Polly R., Rabung T. and Schmidt M. (2013) Mineral-water interface reactions of actinides. *Chemical Reviews* **113**, 1016–1062.
- Guillaumont R. and Mompean F. J. (2003) *Update on the chemical thermodynamics of uranium, neptunium, plutonium, americium and technetium.*, Elsevier Amsterdam.
- Hanna K., Martin S., Quilès F. and Boily J. F. (2014) Sorption of phthalic acid at goethite surfaces under flow-through conditions. *Langmuir* **30**, 6800–6807.
- Henderson P. ed. (1984) *Rare earth element geochemistry.*, Elsevier, Amsterdam ; New York.
- Hiemstra T., De Wit J. C. M. and Van Riemsdijk W. H. (1989) Multisite proton adsorption modeling at the solid/solution interface of (hydr)oxides: A new approach: II. Application to various important (hydr)oxides. *Journal of Colloid and Interface Science* **133**, 105–117.
- Jada A., Ait Akbour R. and Douch J. (2006) Surface charge and adsorption from water onto quartz sand of humic acid. *Chemosphere* **64**, 1287–1295.
- Jin Q., Wang G., Ge M., Chen Z., Wu W. and Guo Z. (2014) The adsorption of Eu(III) and Am(III) on Beishan granite: XPS, EPMA, batch and modeling study. *Applied Geochemistry* **47**, 17–24.
- Kar A. S., Tomar B. S., Godbole S. V. and Manchanda V. K. (2011) Time resolved fluorescence spectroscopy and modeling of Eu(III) sorption by silica in presence and absence of alpha hydroxy isobutyric acid. *Colloids and Surfaces A: Physicochemical and Engineering Aspects* **378**, 44–49.
- Karimzadeh L., Lippold H., Stockmann M. and Fischer C. (2020) Effect of DTPA on europium sorption onto quartz – Batch sorption experiments and surface complexation modeling. *Chemosphere* **239**, 124771.
- Kinniburgh D. G. and Cooper D. M. (2009) PhreePlot: Creating graphical output with PHREEQC.

- Kitamura A., Fujiwara K., Yamamoto T., Nishikawa S. and Moriyama H. (1999) Analysis of Adsorption Behavior of Cations onto Quartz Surface by Electrical Double-layer Model. *Journal of Nuclear Science and Technology* **36**, 1167–1175.
- Klungness G. D. and Byrne R. H. (2000) Comparative hydrolysis behavior of the rare earths and yttrium: the influence of temperature and ionic strength. *Polyhedron* **19**, 99–107.
- Kursun I., Terzi M. and Tombal T. D. (2016) HCl leaching behaviour of a bastnasite ore in terms of thorium and rare earth elements. *Russ. J. Non-Ferrous Metals* **57**, 187–194.
- Langkau S. and Erdmann M. (2020) Environmental impacts of the future supply of rare earths for magnet applications. *Journal of Industrial Ecology*, jiec.13090.
- Li Z., Wei Y., Zhang C., Zhou B. and Zhao Y. (2016) Rare Earth Elements supply vs. clean energy technologies: new problems to be solve. *Gospodarka Surowcami Mineralnymi - Mineral Resources Management; 2016; vol. 32; No 4*.
- Liu W., Etschmann B., Migdisov A., Boukhalfa H., Testemale D., Müller H., Hazemann J.-L. and Brugger J. (2017) Revisiting the hydrothermal geochemistry of europium(II/III) in light of new in-situ XAS spectroscopy results. *Chemical Geology* **459**, 61–74.
- Luo and Byrne R. H. (2001) Yttrium and Rare Earth Element Complexation by Chloride Ions at 25°C. *Journal of Solution Chemistry* **30**, 837–845.
- Luo T., Xu J., Cheng W., Zhou L., Marsac R., Wu T., Boily J.-F. and Hanna K. (2022) Interactions of Anti-Inflammatory and Antibiotic Drugs at Mineral Surfaces Can Control Environmental Fate and Transport. *Environ. Sci. Technol.* **56**, 2378–2385.
- Luo Y.-R. and Byrne R. H. (2004) Carbonate complexation of yttrium and the rare earth elements in natural waters. *Geochimica et Cosmochimica Acta* **68**, 691–699.
- Lützenkirchen J., Marsac R., Kulik D. A., Payne T. E., Xue Z., Orsetti S. and Haderlein S. B. (2015) Treatment of multi-dentate surface complexes and diffuse layer implementation in various speciation codes. *Applied Geochemistry* **55**, 128–137.
- Marsac R., Banik N. L., Lützenkirchen J., Buda R. A., Kratz J. V. and Marquardt C. M. (2015) Modeling plutonium sorption to kaolinite: Accounting for redox equilibria and the stability of surface species. *Chemical Geology* **400**, 1–10.
- Marsac R., Catrouillet C., Davranche M., Bouhnik-Le Coz M., Briant N., Janot N., Otero-Fariña A., Groenenberg J. E., Pédrot M. and Dia A. (2021) Modeling rare earth elements binding to humic acids with model VII. *Chemical Geology* **567**, 120099.
- Marsac R., Davranche M., Gruau G., Bouhnik-Le Coz M. and Dia A. (2011) An improved description of the interactions between rare earth elements and humic acids by modeling: PHREEQC-Model VI coupling. *Geochimica et Cosmochimica Acta* **75**, 5625–5637.

- Marsac R., Davranche M., Gruau G. and Dia A. (2010) Metal loading effect on rare earth element binding to humic acid: Experimental and modelling evidence. *Geochimica et Cosmochimica Acta* **74**, 1749–1761.
- Marsac R., Davranche M., Gruau G., Dia A. and Bouhnik-Le Coz M. (2012) Aluminium competitive effect on rare earth elements binding to humic acid. *Geochimica et Cosmochimica Acta* **89**, 1–9.
- Marsac R., Davranche M., Gruau G., Dia A., Pédrot M., Coz-bouhnik M. L. and Briant N. (2013) Effects of Fe competition on REE binding to humic acid : Origin of REE pattern variability in organic waters. *Chemical Geology* **342**, 119–127.
- Marsac R., Réal F., Banik N. L., Pédrot M., Pourret O. and Vallet V. (2017) Aqueous chemistry of Ce(IV): estimations using actinide analogues. *Dalton Trans.* **46**, 13553–13561.
- Moog H. C., Bok F., Marquardt C. M. and Brendler V. (2015) Disposal of nuclear waste in host rock formations featuring high-saline solutions – Implementation of a thermodynamic reference database (THEREDA). *Applied Geochemistry* **55**, 72–84.
- Nagao S., Rao R. R., Killey R. W. D. and Young J. L. (1998) Migration Behavior of Eu(III) in Sandy Soil in the Presence of Dissolved Organic Materials. *Radiochimica Acta* **82**, 205–212.
- Nair S., Karimzadeh L. and Merkel B. J. (2014) Surface complexation modeling of Uranium(VI) sorption on quartz in the presence and absence of alkaline earth metals. *Environ Earth Sci* **71**, 1737–1745.
- Naveau A., Monteil-Rivera F., Dumonceau J. and Boudesocque S. (2005) Sorption of europium on a goethite surface: influence of background electrolyte. *Journal of Contaminant Hydrology* **77**, 1–16.
- Ohta A. and Kawabe I. (2001) REE(III) adsorption onto Mn dioxide ( $\delta$ -MnO<sub>2</sub>) and Fe oxyhydroxide: Ce(III) oxidation by  $\delta$ -MnO<sub>2</sub>. *Geochimica et Cosmochimica Acta* **65**, 695–703.
- Pack A., Russell S. S., Shelley J. M. G. and van Zuilen M. (2007) Geo- and cosmochemistry of the twin elements yttrium and holmium. *Geochimica et Cosmochimica Acta* **71**, 4592–4608.
- Parkhurst D. L. and Appelo C. A. J. (1999) User's guide to PHREEQC (Version 2): A computer program for speciation, batch-reaction, one-dimensional transport, and inverse geochemical calculations. *Water-resources investigations report* **99**, 312.
- Pitois A., Abrahamsen L. G., Ivanov P. I. and Bryan N. D. (2008) Humic acid sorption onto a quartz sand surface: A kinetic study and insight into fractionation. *Journal of Colloid and Interface Science* **325**, 93–100.
- Pourret O. and Davranche M. (2013) Rare earth element sorption onto hydrous manganese oxide: A modeling study. *Journal of Colloid and Interface Science* **395**, 18–23.
- Powell M. (1965) A method for minimizing a sum of squares of non-linear functions without calculating derivatives. *The Computer Journal* **7**, 303–307.

- Prikryl J. D., Jain A., Turner D. R. and Pabalan R. T. (2001) Uranium(VI) sorption behavior on silicate mineral mixtures. *Journal of contaminant hydrology* **47**, 241–253.
- Quinn K. A., Byrne R. H. and Schijf J. (2004) Comparative Scavenging of Yttrium and the Rare Earth Elements in Seawater: Competitive Influences of Solution and Surface Chemistry. *Aquatic Geochemistry* **10**, 59–80.
- Rabung T., Geckeis H., Kim J.-I. and Beck H. P. (1998) Sorption of Eu(III) on a Natural Hematite: Application of a Surface Complexation Model. *Journal of Colloid and Interface Science* **208**, 153–161.
- Reiller P., Moulin V., Casanova F. and Dautel C. (2003) On the study of Th(IV)-humic acid interactions by competition sorption studies with silica and determination of global interaction constants. *Radiochimica Acta* **91**, 513–524.
- Scheidegger A., Borkovec M. and Sticher H. (1993) Coating of silica sand with goethite: preparation and analytical identification. *Geoderma* **58**, 43–65.
- Schnurr A., Marsac R., Rabung T., Lützenkirchen J. and Geckeis H. (2015) Sorption of Cm(III) and Eu(III) onto clay minerals under saline conditions: Batch adsorption, laser-fluorescence spectroscopy and modeling. *Geochimica et Cosmochimica Acta* **151**, 192–202.
- Shannon R. D. (1976) Revised Effective Ionic Radii and Systematic Studies of Interatomic Distances in Halides and Chalcogenides.
- Šimůnek J., M. Šejna A., Saito H., Sakai M. and Genuchten M. Th. V. (2013) The HYDRUS-1D software package for simulating the movement of water, heat, and multiple solutes in variably saturated media, version 4.17. *HYDRUS Software Series 3D*, 343.
- Stumm W. and Morgan J. J. (1996) *Aquatic Chemistry: Chemical Equilibria and Rates in Natural Waters*, 3rd ed. John Wiley & Sons, Inc., New York,.
- Takahashi Y., Châtellier X., Hattori K. H., Kato K. and Fortin D. (2005) Adsorption of rare earth elements onto bacterial cell walls and its implication for REE sorption onto natural microbial mats. *Chemical Geology* **219**, 53–67.
- Takahashi Y., Tada A., Kimura T. and Shimizu H. (2000) Formation of Outer- and Inner-Sphere Complexes of Lanthanide Elements at Montmorillonite-Water Interface. *Chemistry Letters - CHEM LETT* **29**, 700–701.
- Takahashi Y., Yamamoto M., Yamamoto Y. and Tanaka K. (2010) EXAFS study on the cause of enrichment of heavy REEs on bacterial cell surfaces. *Geochimica et Cosmochimica Acta* **74**, 5443–5462.
- Tang J. and Johannesson K. H. (2005) Adsorption of rare earth elements onto Carrizo sand: Experimental investigations and modeling with surface complexation. *Geochimica et Cosmochimica Acta* **69**, 5247–5261.
- Tang J. and Johannesson K. H. (2010) Rare earth elements adsorption onto Carrizo sand: Influence of strong solution complexation. *Chemical Geology* **279**, 120–133.

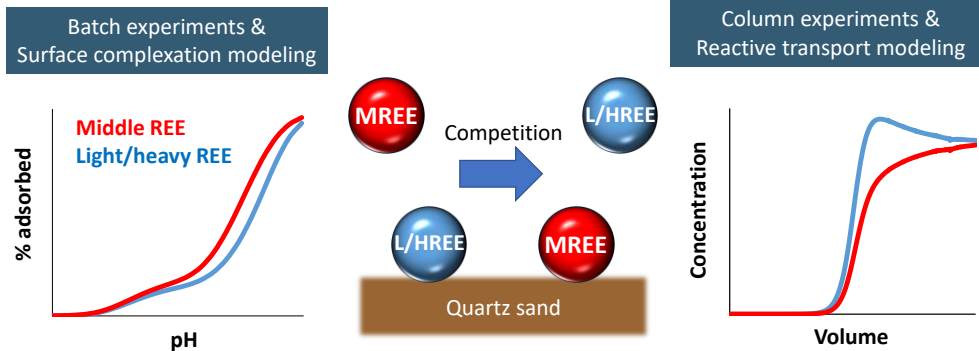
- Turner D. R. and Sassman S. A. (1996) Approaches to sorption modeling for high-level waste performance assessment. *Journal of Contaminant Hydrology* **21**, 311–332.
- Wang Y., Wan Q., Liu B., Wei Z., Zhang M. and Tang Y. (2020) Co-transport and competitive retention of different ionic rare earth elements (REEs) in quartz sand: Effect of kaolinite. *Science of The Total Environment* **722**, 137779.
- Warwick P. W., Hall A., Pashley V., Bryan N. D. and Griffin D. (2000) Modelling the effect of humic substances on the transport of europium through porous media: a comparison of equilibrium and equilibrium/kinetic models. *Journal of Contaminant Hydrology* **42**, 19–34.
- Wu J., Zhao X., Li Z. and Gu X. (2020) Thermodynamic and kinetic coupling model of Cd(II) and Pb(II) adsorption and desorption on goethite. *Science of The Total Environment* **727**, 138730.
- Xu J., Marsac R., Wei C., Wu F., Boily J.-F. and Hanna K. (2017) Co-binding of Pharmaceutical Compounds at Mineral Surfaces: Mechanistic Modeling of Binding and Co-binding of Nalidixic Acid and Niflumic Acid at Goethite Surfaces. *Environmental Science & Technology* **51**, 11617–11624.
- Yeghicheyan D., Aubert D., Bouhnik-Le Coz M., Chmeleff J., Dupoux S., Djouraev I., Granier G., Lacan F., Piro J., Rousseau T., Cloquet C., Marquet A., Menniti C., Pradoux C., Freydier R., Vieira da Silva-Filho E. and Suchorski K. (2019) A New Interlaboratory Characterisation of Silicon, Rare Earth Elements and Twenty-Two Other Trace Element Concentrations in the Natural River Water Certified Reference Material SLRS -6 ( NIST - CNRC ). *Geostand Geoanal Res* **43**, 475–496.
- Yoshida T. and Suzuki M. (2006) Migration of strontium and europium in quartz sand column in the presence of humic acid: Effect of ionic strength. *J Radioanal Nucl Chem* **270**, 363–368.
- Zavarin M., Chang E., Wainwright H., Panamir N., Kaukuntla R., Zouabe J., Deinhart A., Genetti V., Shipman S., Bok F. and Brendler V. (2022) Community Data Mining Approach for Surface Complexation Database Development. *Environ. Sci. Technol.* **56**, 2827–2838.
- Zhou L., Cheng W., Marsac R., Boily J.-F. and Hanna K. (2022) Silicate surface coverage controls quinolone transport in saturated porous media. *Journal of Colloid and Interface Science* **607**, 347–356.
- Zoll A. M. and Schijf J. (2012) A surface complexation model of YREE sorption on *Ulva lactuca* in 0.05–5.0M NaCl solutions. *Geochimica et Cosmochimica Acta* **97**, 183–199.

**Declaration of interests**

The authors declare that they have no known competing financial interests or personal relationships that could have appeared to influence the work reported in this paper.

Journal Pre-proof

## Graphical abstract



Journal Pre-proof